

# Contour forward flux sampling: Sampling rare events along multiple collective variables

Ryan S. DeFever and Sapna Sarupria\*  
*Department of Chemical & Biomolecular Engineering  
Clemson University, Clemson, SC 29634*

Many rare event transitions involve multiple collective variables (CVs) and the most appropriate combination of CVs is generally unknown a priori. We thus introduce a new method, contour forward flux sampling (cFFS), to study rare events with multiple CVs simultaneously. cFFS places nonlinear interfaces on-the-fly from the collective progress of the simulations, without any prior knowledge of the energy landscape or appropriate combination of CVs. We demonstrate cFFS on analytical potential energy surfaces and a conformational change in alanine dipeptide.

## I. INTRODUCTION

Rare events remain uniquely challenging to study in molecular simulations.[1] These infrequent transitions between long-lived (meta)stable states are characterized by large differences between the timescales of the relevant physics (e.g., molecular vibrations, hydrogen bond lifetimes, etc.) and the time between events (often  $\mu$ s to s). Exemplars include crystal nucleation[2–5], ion-pair dissociation in solution,[6, 7] conformational changes in biomolecules[8, 9], and chemical reactions[10]. Due to the prevalence and importance of rare events, several advanced sampling methods have been developed[11–21] to estimate transition rate constants and sample unbiased trajectories connecting the stable states. However, even with increasing computational power some phenomena remain challenging to study and continued method development is required.

We present contour forward flux sampling (cFFS), a novel method to sample rare events with multiple collective variables[22] (CVs) simultaneously. Building on forward flux sampling (FFS), cFFS leverages overall trajectory behavior to on-the-fly determine nonlinear interface placement in multiple CVs. FFS is a rare event sampling method that uses a series of non-overlapping interfaces to drive a system from an initial state  $A$  to final state  $B$ . [15, 16, 23, 24] Each interface is defined by some value of an order parameter,  $\lambda$ , which changes monotonically from  $A$  to  $B$ . Straightforward simulation in  $A$  is used to estimate the flux,  $\Phi_{A0}$ , from  $A$  to the first interface,  $\lambda_0$ , and to collect a large number of first-crossing phase points at  $\lambda_0$ . The designation of a phase point as a first-crossing point indicates that upon following the trajectory backwards in time from the point, one would reach  $\lambda_A$  before  $\lambda > \lambda_0$ . Several trajectories are initiated from each phase point collected at  $\lambda_0$  ( $\lambda_i$ ). Stochasticity from the dynamics or velocity perturbation at the start of each simulation ensures trajectory divergence. Trajectories returning to  $A$  are discarded, while those reaching the next interface,  $\lambda_1$  ( $\lambda_{i+1}$ ), are stored for the next iteration. This procedure is re-

peated for each interface until the boundary of  $B$  is reached, or the probability of advancing to the next interface,  $P(\lambda_{i+1}|\lambda_i)$ , plateaus to 1. The transition rate constant is calculated as  $k_{AB} = \Phi_{A0} \prod_{i=0}^{n-1} P(\lambda_{i+1}|\lambda_i)$  and transition paths from  $A$  to  $B$  are generated by connecting the partial paths backward from  $B$  to  $A$ . FFS has emerged as a popular choice for studying rare events in simulation because it is applicable to equilibrium and nonequilibrium systems, and implementation is algorithmically straightforward and embarrassingly parallel.

Despite its advantages, FFS has shortcomings. Assuming reasonable definitions for the boundaries of  $A$  and  $B$ , the rate constant and transition path ensemble (TPE) computed with FFS are, in principle, independent of the order parameter used for the calculation.[16] In practice, a poor choice of order parameter is detrimental to the efficiency of FFS[25, 26] and can even lead to incorrect results.[26, 27] This arises when portions of  $\lambda_i$  which are important to the transition are sparingly sampled. More formally, imagine some coordinate ( $\lambda^\perp$ ) orthogonal to  $\lambda$ . Challenges arise for FFS when there is poor overlap between the distribution of first-crossing phase points captured at  $\lambda_i$ ,  $\rho(\lambda^\perp|\lambda_i)$ , and the probability of reaching  $\lambda_B$  from some point on  $\lambda_i$ ,  $P(\lambda_B|\lambda_i; \lambda^\perp)$ . [26] There are two approaches to overcome this issue: (1) increase sampling to collect more phase points at problematic interface(s), or (2) improve the choice of order parameter to increase overlap between the two distributions. The first approach yields more phase points everywhere along an interface, but with sufficient sampling the paths spawned from phase points with a higher  $P(\lambda_B|\lambda_i; \lambda^\perp)$  will come to dominate the eventual path ensemble, resulting in the correct rate constant and TPE. Unfortunately, the efficiency of FFS will still be poor. In contrast, the second approach increases the efficiency of FFS, meaning that FFS will converge to the correct rate constant and TPE with less sampling. Unfortunately, optimal order parameters are rarely known a priori. More often, one of the reasons for generating a path ensemble with a method such as FFS is to identify order parameters which best describe the transition.

Since sampling of all interfaces  $i > 0$  in FFS depends on the phase points collected at  $\lambda_0$ , methods have been proposed to optimize placement of, and

arXiv:1901.03422v1 [cond-mat.stat-mech] 10 Jan 2019

\* ssarupr@g.clemson.edu

ensure adequate sampling of  $\lambda_0$ . [2, 28, 29] If the situation is not too dire, increasing the length of the basin simulation and collecting more phase points at  $\lambda_0$  may provide a sufficient remedy. However, if overlap between  $\rho(\lambda^\perp|\lambda_0)$  and  $P(\lambda_B|\lambda_0; \lambda^\perp)$  is extremely small, this may be insufficient. Furthermore, the problem is not limited to  $\lambda_0$ ; in principle the distribution of phase points sampled at any  $\lambda_i$  could suffer from this problem. Poor overlap between  $\rho(\lambda^\perp|\lambda_i)$  and  $P(\lambda_B|\lambda_i; \lambda^\perp)$  becomes particularly problematic for systems with multiple transition tubes. There, a poor choice of order parameter may result in some transition tubes becoming (artificially) favored over others. In the extreme, entire transition tubes can be missed by FFS.

A related situation worth mentioning is when  $\rho(\lambda^\perp|\lambda_0)$  converges extremely slowly. [2, 29] If this is the problem, extending the basin simulations until convergence is achieved will remedy the situation. [2] A greater number of phase points at  $\lambda_0$  are not required; just phase points correctly sampled from the converged distribution.

The choice of order parameter strongly affects the overlap between  $\rho(\lambda^\perp|\lambda_i)$  and  $P(\lambda_B|\lambda_i; \lambda^\perp)$ . If the order parameter is the committor function,  $P(\lambda_B|\lambda_i; \lambda^\perp)$  is constant with  $\lambda^\perp$ , thereby assuring good overlap between  $\rho(\lambda^\perp|\lambda_i)$  and  $P(\lambda_B|\lambda_i; \lambda^\perp)$ . [26] Borrero and Escobedo thus devised a method to optimize the order parameter with a series of FFS simulations. [30] Though the approach yields improvements [9], it is challenging for systems which require extraordinary computational resources for even a single FFS run. [4, 5] Furthermore, some processes are inherently multidimensional, [6, 31–33] and driving the transition along a single CV may not be ideal.

cFFS takes a different approach. We extend FFS to use multiple CVs on-the-fly. This allows researchers to test multiple CVs simultaneously and improves the chances of capturing important orthogonal coordinates within the set of CVs used to drive the transition. At each interface, cFFS identifies the next interface as a nonlinear combination of specified CVs on-the-fly from the behavior of simulations initiated from the previous interface. In doing so, cFFS also reveals the role of each CV through the entire transition. Only the combination of CVs must separate  $A$  and  $B$  and so each CV need not monotonically change from  $A$  to  $B$ . If some CV is unimportant, this will be reflected by, but not impede cFFS. These features offer substantial flexibility in CVs that can be used with cFFS. cFFS generates an estimate of the transition rate constant and a collection of  $A \rightarrow B$  trajectories belonging to the TPE. We demonstrate cFFS with two CVs, but in principle it can be extended to three or more CVs.

In Sec. II we explain cFFS. We proceed to demonstrate cFFS on several two-dimensional potential energy surfaces in Sec. III. In Sec. IV, we demonstrate cFFS with one position coordinate and one momentum coordinate, and in Sec. V we test cFFS on a

standard higher dimensional test case, a conformational transition in alanine dipeptide. Discussion and closing remarks are provided in Sec. VI and Sec. VII, respectively.

## II. CONTOUR FORWARD FLUX SAMPLING

The central idea of cFFS is to allow the system to naturally evolve along multiple CVs to reveal how different CVs participate in the transition. This is achieved by placing the subsequent interface based on sampling initiated from the current interface. The FFS formalism can still be used to calculate the rate constant and TPE. Interface placement is designed such that the distribution of first-crossing points is uniform along the interface, ensuring that each interface is well-sampled everywhere within the chosen CVs.

The first step of cFFS is to run straightforward basin simulations in  $A$  to identify the bounds of  $A$  ( $\lambda_A$ ) and the first interface ( $\lambda_0$ ), and to collect phase points at  $\lambda_0$ . The value of each CV in time,  $\boldsymbol{\lambda}(t)$ , is calculated, where  $\boldsymbol{\lambda} \equiv \{\lambda^I, \lambda^{II}, \dots, \lambda^N\}$  is the set of CVs. CV space is discretized to create an  $N$ -D grid. The discretization size is selected such that the system rarely travels more than a single grid site in one time step. The discrete probability distribution,  $P(\boldsymbol{\lambda})$ , is calculated from the basin simulations. Grid sites exceeding a threshold probability are added to the set of sites describing  $A$ ,  $\mathbf{s}_A$ . Regions of CV space which are not in  $\mathbf{s}_A$  but completely surrounded by  $\mathbf{s}_A$  are added to  $\mathbf{s}_A$ .  $\lambda_A$  is defined as the boundary between sites in  $\mathbf{s}_A$  and those that are not. Trajectories exit  $A$  when they cross from a grid site in  $\mathbf{s}_A$  to a grid site not in  $\mathbf{s}_A$ .

Several criteria are used to identify  $\mathbf{s}_0$ , the set defining  $\lambda_0$ .  $\mathbf{s}_0$  should: (a) completely contain  $\mathbf{s}_A$  so that  $\lambda_0$  does not overlap with or cross  $\lambda_A$ , (b) not create regions of CV space completely surrounded by  $\mathbf{s}_0$ , but not included in it, (c) not include sites in  $\mathbf{s}_B$ , the set of sites describing  $B$ , (d) be selected such that some desired number of phase points can be collected at  $\lambda_0$ , and (e) be selected such that there is equal flux of trajectories exiting  $\mathbf{s}_0$  along the entire  $\lambda_0$  interface. Criteria (e) is crucial as it ensures that cFFS does not bias the system to sample any one direction more readily than another. Further discussion is provided later. Once  $\lambda_A$  and  $\lambda_0$  are defined the basin simulations are re-analyzed to calculate  $\Phi_{A0}$  and collect phase points at  $\lambda_0$ .

The remainder of cFFS proceeds as follows. Several trajectories are initiated from each phase point at  $\lambda_i$  ( $\lambda_i = \lambda_0$  for the first iteration). Trajectories are terminated when they return to  $\lambda_A$ , or reach a maximum number of steps. The set of sites defining  $\lambda_{i+1}$ ,  $\mathbf{s}_{i+1}$ , is determined from the behavior of trajectories initiated at  $\lambda_i$  using analogous criteria to those described for determining  $\lambda_0$ . Note that  $\mathbf{s}_{i+1}$  must completely contain  $\mathbf{s}_i$  to satisfy the effective positive flux formalism. [14, 34] Once  $\mathbf{s}_{i+1}$  is identified, trajec-

tories are re-analyzed to determine if they cross  $\lambda_{i+1}$  (i.e., exit  $\mathbf{s}_{i+1}$ ) before returning to  $A$ . For each trajectory that crosses  $\lambda_{i+1}$ , the phase point at the time step which the trajectory crosses  $\lambda_{i+1}$  is saved. Trajectories which fail to reach  $\lambda_{i+1}$  or return to  $A$  before the maximum number of steps are extended until they reach  $\lambda_{i+1}$  or return to  $A$ . The probability,  $P(\lambda_{i+1}|\lambda_i)$ , is calculated from the number of trajectories that reach  $\lambda_{i+1}$  before returning to  $A$ .

Eventually, sites in  $\mathbf{s}_{i+1}$  will be adjacent to sites in  $\mathbf{s}_B$ . Trajectories initiated from  $\lambda_i$  can then reach  $\lambda_{i+1}$ , return to  $A$ , or proceed directly to  $B$ . This indicates the kinetic barrier has been surmounted and thus cFFS is nearly complete. Two probabilities are now calculated;  $P(\lambda_{i+1}|\lambda_i)$  and  $P(\lambda_B|\lambda_i)$ . Our approach is to continue cFFS until  $\mathbf{s}_{i+1}$  surrounds  $\mathbf{s}_B$ . At this point,  $i$  becomes the final interface,  $n$ . Trajectories initiated from  $\lambda_n$  are continued until they reach  $\lambda_B$  or return to  $\lambda_A$  to close the probabilities for the rate calculation. As with multi-state FFS[35], the transition rate constant is calculated as

$$k_{AB} = \Phi_{A0} \sum_{j=0}^n P(\lambda_B|\lambda_j) \prod_{i=0}^{j-1} P(\lambda_{i+1}|\lambda_i). \quad (1)$$

The collection of trajectories comprising the TPE is constructed by connecting the partial paths backwards from  $B$  to  $A$ . Note that all trajectories *do not* have equal weight in the TPE. The relative weight of each trajectory is  $w = 1/\prod_{i=0}^j k_i$ , where  $j$  is the final interface crossed by a trajectory before reaching  $B$  and  $k_i$  is the number of trajectories initiated from each configuration at interface  $i$ .

### III. DEMONSTRATION ON 2D POTENTIAL ENERGY SURFACES

We demonstrate cFFS with Langevin dynamics of a single particle on four 2D potential energy surfaces (PESs) with different topographical features (see Fig. 1(a)–(d)). PES-1 has a single transition tube which follows two monotonically increasing CVs. PES-2 has a single transition tube with hysteresis in the  $x$  coordinate. PES-3 and PES-4 both contain two transition tubes; the potential energy barriers are the same for the two tubes on PES-3, and different for the two tubes on PES-4. For each PES, we study  $A \rightarrow B$  transitions with straightforward Langevin dynamics (SLD), FFS<sub>opt</sub>, FFS<sub>x</sub>, and cFFS. FFS<sub>opt</sub> denotes FFS performed with the optimal linear combination of  $x$  and  $y$  (i.e., the order parameter orthogonal to the dividing surface of the PES), and FFS<sub>x</sub> indicates FFS performed with  $x$  as the (suboptimal) order parameter. We stress that optimal order parameters are not known a priori for most realistic systems, and therefore FFS is generally performed with suboptimal order parameters. Further details of the PESs, Langevin dynamics, and FFS/cFFS parameters are provided in the Supporting Information (SI).

#### A. Rate constants

TABLE I.  $A \rightarrow B$  transition rate constants for four 2D PESs. One standard deviation of the mean is reported in parenthesis.

PES	$k_{AB} \times 10^5$ at $\beta = 2.5$			
	SLD	FFS <sub>opt</sub>	FFS <sub>x</sub>	cFFS
PES-1	2.9 (0.2)	2.8 (0.3)	3.1 (0.9)	2.8 (0.2)
PES-2	9.1 (0.1)	7.9 (0.9)	10.2 (2.5)	8.8 (0.7)
PES-3	2.6 (0.3)	2.4 (0.4)	2.3 (0.6)	2.4 (0.1)
PES-4	1.1 (0.1)	1.0 (0.1)	1.1 (0.1)	1.0 (0.1)
$k_{AB} \times 10^9$ at $\beta = 5.0$				
PES-1	5.4 (1.2)	4.4 (0.2)	3.1 (0.2)	4.5 (0.6)
PES-2	23.2 (2.0)	18.0 (3.5)	18.3 (1.0)	21.9 (2.3)
PES-3	6.4 (1.3)	2.9 (0.2)	2.5 (0.2)	5.4 (0.5)
PES-4	2.8 (0.9)	1.9 (0.4)	0.42 (0.02)	2.6 (0.1)

$A \rightarrow B$  transition rate constants are reported in Table I. Transitions were studied at  $\beta = 2.5$  and  $\beta = 5.0$  ( $\beta = 1/k_B T$ ). The higher temperature ( $\beta = 2.5$ ) enables rigorous comparison of TPE sampling with SLD, whereas the lower temperature ( $\beta = 5.0$ ) provides a test at more challenging conditions. SLD rate constants are unbiased estimates. FFS<sub>x</sub> provides accurate estimates of the rate constants at  $\beta = 2.5$ , but at  $\beta = 5.0$  FFS<sub>x</sub> underestimates the rate constants. This suggests that suboptimal order parameters perform worse as the barrier becomes larger relative to  $k_B T$ . We explain the breakdown of FFS<sub>x</sub> by examining the TPE sampling below. FFS<sub>opt</sub> and cFFS perform better. Rate constants from FFS<sub>opt</sub> and cFFS both agree nicely with SLD at  $\beta = 2.5$ . At  $\beta = 5.0$ , FFS<sub>opt</sub> underestimates rate constants for PES-2 and PES-3. In contrast, cFFS provides correct estimates of the rate constants for all four PESs at  $\beta = 5.0$ .

#### B. Transition path ensemble sampling

Though attaining the correct  $A \rightarrow B$  rate constant is a crucial test of cFFS, it is also important that cFFS correctly samples the TPE. TPE sampling is calculated as  $\langle \rho \rangle_{\text{TP}} = \langle n_{\text{visits}}/l^2 \rangle_{\text{TP}}$ , where  $\langle \dots \rangle_{\text{TP}}$  indicates an ensemble average over all transition paths, and  $n_{\text{visits}}$  is the number of times a transition path visited each  $l \times l$  region of space. For reference, TPE sampling from SLD at  $\beta = 2.5$  is shown in the bottom panels of Fig. 1.

Fig. 2 summarizes the behavior of FFS<sub>opt</sub>, FFS<sub>x</sub>, and cFFS on PES-1–PES-4 at  $\beta = 5.0$ . All methods result in qualitatively similar sampling for PES-1. The other surfaces proved more challenging for FFS<sub>x</sub> and FFS<sub>opt</sub>. In contrast, cFFS results in the qualitatively correct sampling for all four PESs. On PES-2, the hysteresis provides a challenge for FFS<sub>x</sub>. Unlike FFS<sub>opt</sub> and cFFS, FFS<sub>x</sub> undersamples the  $x < 0$  portion of the transition tube. On PES-3 and PES-4, the failure of FFS<sub>x</sub> is even more stark; FFS<sub>x</sub> only samples

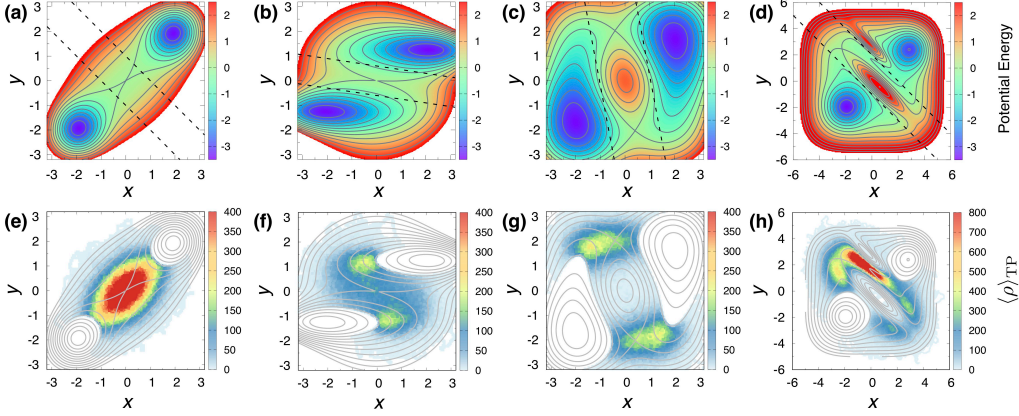


FIG. 1. *Top panels*: PESs used to test cFFS: (a) PES-1, (b) PES-2, (c) PES-3, and (d) PES-4. Color represents the potential energy. Contour lines are separated by 0.5 units. The region between the dashed lines was used to quantitatively compare  $\rho(q|TP)$  between different methods. *Bottom panels*: TPE sampling from SLD at  $\beta = 2.5$  on (e) PES-1, (f) PES-2, (g) PES-3, and (h) PES-4.

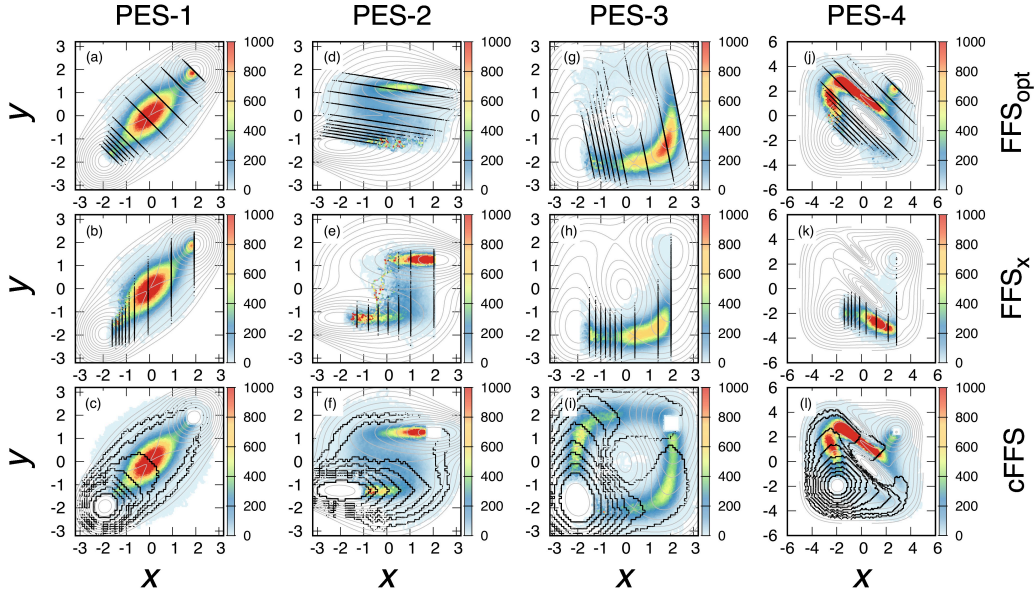


FIG. 2. Comparison of interface placement and TPE sampling generated with  $FFS_{opt}$ ,  $FFS_x$ , and cFFS on PES-1 – PES-4 at  $\beta = 5.0$ . PES contours are shown as gray lines. Configurations collected at each interface are shown with black points. TPE sampling represented by the heatmap.

one of the two transition tubes. Even  $FFS_{opt}$  fails to sample both transition tubes equally on PES-3. PES-3 and PES-4 have two distinct transition tubes, and the minimum energy paths change direction from  $A$  to  $B$ . On PES-3, both transition tubes have the same potential energy barrier. However, one transition tube approaches the transition state from  $A$  with a gentler slope. Results from SLD at  $\beta = 2.5$  in Fig. 1(c) indicate that both transitions should be equally traveled. cFFS reproduces this behavior at both  $\beta = 2.5$  (SI Fig. S1) and the more challenging  $\beta = 5.0$  (Fig. 2(i)). At  $\beta = 5.0$ ,  $FFS_x$  only samples a single transition tube (Fig. 2(h)). Even  $FFS_{opt}$  struggles to sample

both transition tubes equally on PES-3 (Fig. 2(g)). The behavior of  $FFS_{opt}$  and  $FFS_x$  on PES-3 can be explained by the framework put forth in the introduction. In both cases, it is apparent that  $\rho(\lambda^\perp|\lambda_0)$  sampled during the basin simulations only has good overlap with  $P(\lambda_B|\lambda_0;\lambda^\perp)$  for one of the two transition tubes. The result is that FFS oversamples the tube with greater overlap, at the expense of the other transition tube. FFS sensitivity to the choice of order parameter on PES-3 is further demonstrated in SI Fig. S2. Though FFS will converge to the correct TPE in the limit of infinite sampling, as a practical matter FFS can lead to incorrect results. cFFS again

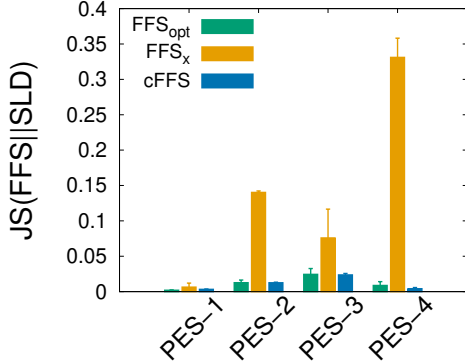


FIG. 3. Jensen-Shannon divergence between  $\rho(q|TP)$  calculated with SLD and FFS<sub>opt</sub>, FFS<sub>x</sub>, and cFFS at  $\beta = 2.5$ . A value of zero indicates identical probability distributions, while a value of 1.0 indicates completely non-overlapping distributions. Error bars represent one standard deviation on the mean of three independent trials.

performs well on PES-4, illustrating that cFFS is able to navigate a tortuous transition landscape with two transition tubes and unequal potential energy barriers.

Near the dividing surface (see Fig. 1) we quantitatively compare the TPE density of states,  $\rho(q|TP)$ , from SLD with that from FFS<sub>opt</sub>, FFS<sub>x</sub>, and cFFS using the Jensen-Shannon divergence[36]. We restrict our comparison to  $\beta = 2.5$ , where a large number of transitions can be generated with SLD, hence providing a robust reference. The results shown in Fig. 3 confirm qualitative conclusions from Fig. 2 ( $\beta = 5.0$ ) and SI Fig. S1 ( $\beta = 2.5$ ). At  $\beta = 2.5$ , FFS<sub>opt</sub> and cFFS perform similarly. For the simplest case (PES-1), FFS<sub>x</sub> performs nearly as well as FFS<sub>opt</sub> and cFFS. However, for the more complex surfaces, including the surface with hysteresis (PES-2), and surfaces with two transition tubes (PES-3, PES-4), FFS<sub>x</sub> performs notably worse.

### C. cFFS interface placement

Fig. 2 also demonstrates cFFS interface placement. Interfaces are spaced further apart in directions that trajectories more readily advance and closer together in directions that trajectories struggle to advance. For these low-dimensional systems, interface locations adhere closely to the contours of the PESs. We strongly emphasize that no knowledge of the PES is employed; cFFS places interface  $\lambda_{i+1}$  from the progress of trajectories initiated from  $\lambda_i$  alone.

If not done properly, performing FFS with multiple CVs simultaneously can bias the system to over-sample or under-sample regions of CV space. The amount of work performed by FFS is related to interface spacing (i.e.,  $\lambda_{i+1} - \lambda_i$ ), slope of the free energy landscape between  $\lambda_i$  and  $\lambda_{i+1}$ , and the number of trajectories initiated from  $\lambda_i$ . If the slope of the free energy landscape between two interfaces becomes

steeper,  $\lambda_{i+1}$  is moved closer to  $\lambda_i$  or the number of trajectories initiated from  $\lambda_i$  is increased. Multiple CVs introduces a new prospect; that unequal amounts of work are inserted along different CVs, biasing the system to over-sample in the direction that more work is inserted.

We introduced a condition of constant flux along an interface in cFFS interface placement to address this problem. The force exerted by the underlying free energy surface is proportional to  $-dn_{\text{cross}}/d\lambda$ , where  $n_{\text{cross}}$  is the number of trajectories crossing an interface placed at some value of  $\lambda$ . If  $n_{\text{cross}}$  changes more quickly with changing  $\lambda$ , then the underlying surface must have a steeper slope. Applying the differential definition of work,  $dW = Fd\lambda$ , and thus  $dW \propto dn_{\text{cross}}$  and  $W \propto n_{\text{cross}}$ . Constant flux along the interface requires that all small sections of  $\lambda_{i+1}$  have approximately the same number of trajectories crossing them. This condition ensures that equal work is inserted everywhere along the interface (i.e., in all directions) and results in  $\lambda_{i+1}$  closer to  $\lambda_i$  in directions trajectories struggle to advance and further from  $\lambda_i$  in directions trajectories readily advance. The fact that cFFS is able to reproduce the correct TPE symmetry for PES-3 and PES-4 provides strong evidence that the constant flux along the interface condition is correct.

In complex systems, the optimal order parameter is often expected to be a combination (linear or nonlinear) of multiple (suboptimal) order parameters. This combination is generally nonintuitive and difficult to predict. As such, most applications of FFS use a sub-optimal order parameter (e.g., FFS<sub>x</sub>). On the four PESs, cFFS successfully produces correct TPE sampling without knowing how  $x$  and  $y$  should be combined. Though  $x$  and  $y$  are part of the optimal order parameter, independently,  $x$  and  $y$  are suboptimal order parameters. This suggests that cFFS can outperform FFS when multiple suboptimal order parameters are known, but the optimal order parameter remains unknown. In addition, nonlinear combinations of CVs have increased degeneracy compared with linear combinations of CVs in creating reaction coordinates (i.e., optimal order parameters).[37] Since cFFS interfaces are arbitrarily complex combinations of the specified CVs, there may be substantial flexibility in selecting good CVs for cFFS. A variety of approaches have been proposed for identifying important CVs for rare event transitions.[30, 38–44] For example, recent work suggests that important CVs can be identified from local fluctuations in the (meta)stable basins.[45] We envision using such approaches to identify key CVs for cFFS.

## IV. CFFS WITH A MOMENTUM COORDINATE

FFS is most often applied in the diffusive limit and the CVs used as FFS order parameters are generally only functions of the atomic coordinates. In this sec-

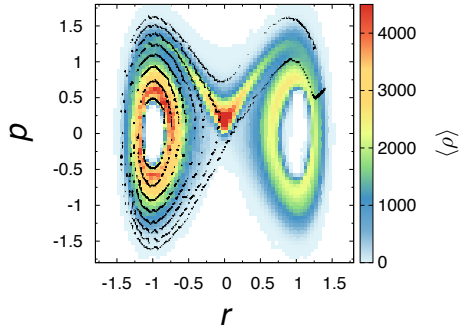


FIG. 4. cFFS on 1D potential with one position coordinate ( $r$ ) and one momentum coordinate ( $p$ ). Initial basin  $A$  is  $r < 0$  minima and final basin  $B$  is  $r > 0$  minima. Configurations collected at each interface are shown as black points. Color map shows the TPE sampling.

tion, we demonstrate cFFS on a simple analytical potential where momentum plays a key role during the transition. A previous study shows that FFS fails and under-predicts the transition rate constant when using a position-based order parameter alone.[26]

Ref. 26 tested several path sampling methods for a transition on a simple 1D analytical potential described by  $V(r) = r^4 - 2r^2$ . Of the tested methods, replica exchange transition interface sampling (RETIS) and partial path transition interface sampling (PPTIS) provided the best estimates to the reference effective positive flux (EPF) rate ( $k_{AB}^{\text{EPF}} = 2.4 \pm 0.1 \times 10^{-7}$ ,  $k_{AB}^{\text{RETIS}} = 2.8 \pm 0.7 \times 10^{-7}$ ,  $k_{AB}^{\text{PPTIS}} = 2.7 \pm 0.6 \times 10^{-7}$ ). FFS performed worst, underestimating the rate constant by 1–2 orders of magnitude depending on the length of the basin simulation. With a basin simulation of 4 million steps, FFS produced a rate constant of  $k_{AB}^{\text{FFS-short}} = 2.2 \pm 0.2 \times 10^{-9}$ . When the basin simulation was extended to 10 million steps,  $k_{AB}^{\text{FFS-long}} = 1.2 \pm 0.1 \times 10^{-8}$ . As explained in Ref. 26, the source of systematic error in the rate constant was the lack of overlap between  $\rho(\lambda^\perp|\lambda_0)$  and  $P(\lambda_B|\lambda_0; \lambda^\perp)$ . Successful transitions require large momentum when exiting the initial basin, and few to none of the trajectories captured at  $\lambda_0$  had the requisite momentum. Even successful transition paths from FFS exited the initial state with lower momenta compared with other methods, resulting in a low estimate of the rate constant. This also resulted in the unphysical result that the momenta of transition paths from FFS were not symmetric about the barrier.

We perform cFFS with the above potential at identical conditions as Ref. 26. The two variables for cFFS are the position ( $r$ ) and momenta ( $p$ ). The basin simulation is performed with 4 million steps. We place interfaces adaptively, collecting  $\sim 2,000$  configurations per interface. As in Ref. 26, we initiate 20,000 trajectories from each interface. cFFS resulted in shooting from 8 interfaces, compared with the 7 interfaces used in Ref. 26. The average rate constant from three cFFS trials was  $k_{AB}^{\text{cFFS}} = 2.0 \pm 0.1 \times 10^{-7}$ , slightly underestimating the EPF rate constant from

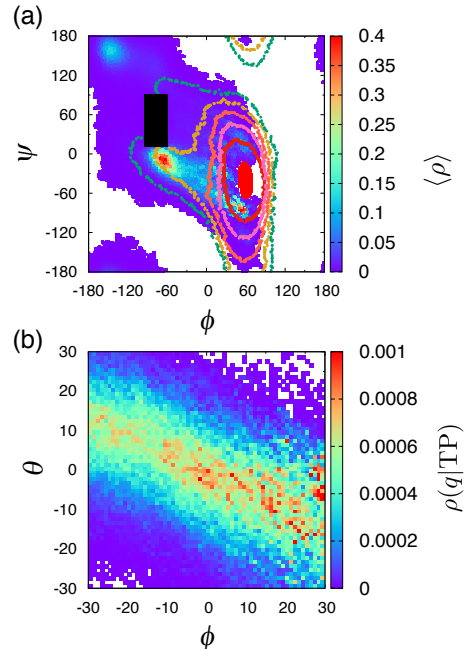


FIG. 5. cFFS for alanine dipeptide in vacuum. (a) Initial and final states are shown as red and black regions, respectively. Configurations collected at  $\lambda_0$ ,  $\lambda_1$ ,  $\lambda_2$ ,  $\lambda_3$ , and  $\lambda_4$  are reported as red, pink, salmon, gold, and green points, respectively. Color map represents the TPE sampling.  $\phi$  and  $\psi$  angles are reported in degrees. (b) Correlation between  $\phi$  and  $\theta$  in the TPE. Color map represents the TPE density of states.

Ref. 26. The TPE and configurations collected at each interface from cFFS are shown in Fig. 4. Paths exit the initial state orbiting the basin and acquiring more kinetic energy until they are able to escape. Their momenta then approaches zero as they cross through the transition state, before accelerating towards and orbiting into the final state. Consistent with theoretical expectations, the TPE generated by cFFS is symmetric about the barrier. We also tested cFFS with less sampling. Even with a twenty-fold reduction in sampling (1000 trajectories, 100 configurations per interface), the rate constant calculated with cFFS is  $k_{AB}^{\text{cFFS}} = 2.6 \pm 0.7 \times 10^{-7}$  and the TPE remains symmetric about the barrier.

These results demonstrate the potential for using cFFS to study transitions with important momenta variables. Though the above test case represents an extremely simple analytical model, it demonstrates the advantages of cFFS in such scenarios. If an important momenta variable is known for a transition, cFFS allows the basins to be separated with a position coordinate and the momentum coordinate can be used to help drive the transition.

## V. DEMONSTRATION ON ALANINE DIPEPTIDE

In keeping with tradition, we close by demonstrating cFFS on the  $C_{7ax}$ -to- $C_{7eq}$  conformational change in alanine dipeptide in vacuum. Details of the simulations and cFFS are reported in the SI.  $\phi$  and  $\psi$  backbone dihedral angles were used as CVs for cFFS. The progression of cFFS is shown in Fig. 5(a). Starting from the  $C_{7ax}$  basin centered near  $\phi = 60^\circ$  and  $\psi = -30^\circ$ , cFFS drives the system to the  $C_{7eq}$  basin defined by  $-94^\circ < \phi < -60^\circ$  and  $12^\circ < \psi < 90^\circ$ . The shape of the interfaces shows that  $\phi$  plays the larger role in the transition and reveals the location of the primary transition tube. The transition rate constant predicted by cFFS ( $k_{AB}^{cFFS} = 5.0 \times 10^6 \text{ s}^{-1}$ ) compares favorably with straightforward simulation ( $k_{AB}^{SLD} = 4.8 \times 10^6 \text{ s}^{-1}$ ). In Fig. 5(b) we show the relationship between  $\phi$  and another dihedral angle,  $\theta$ , in the TPE. It has been shown that  $\theta$  is part of the reaction coordinate[17, 46]. cFFS captures the proper relationship between  $\phi$  and  $\theta$  even though  $\theta$  is not one of the CVs used during cFFS.[17, 19]

## VI. DISCUSSION

cFFS helps overcome a few challenges posed by FFS. cFFS allows one to try multiple CVs simultaneously. This is beneficial for systems where investigators have some a priori insight into the CVs that are expected to play a role in the transition, but a detailed analysis of the mechanism is missing and the best order parameter remains unknown. By using multiple CVs simultaneously and enforcing constant flux along an interface, the method can alleviate issues associated with poor overlap between  $\rho(\lambda^\perp|\lambda_i)$  and  $P(\lambda_B|\lambda_i; \lambda^\perp)$ . Of course, it is possible that there are additional important orthogonal coordinates beyond the chosen CVs. This situation could pose sampling challenges for cFFS. Finally, we demonstrated cFFS with a combination of momenta and position based coordinates. This may extend the practical applicability of FFS to more ballistic systems. FFS depends on stochasticity for trajectory divergence between subsequent interfaces, so it will still not be applicable in the limit of fully deterministic dynamics.

cFFS can in principle be extended to a large number of CVs. However, we surmise the method will not scale well to more than three or four CVs. In high dimensional space, the area through which trajectories can cross an interface will become exceedingly large. From a practical standpoint, this will make it difficult to maintain the constant flux condition. From an efficiency standpoint, most of each interface will drive the system towards regions of phase space which are irrelevant to the transition of interest. Even if successful transitions are generated, they will probably originate from a tiny subset of the phase points collected at  $\lambda_0$  and thus be highly correlated. Challenges associated with scaling to large numbers

of CVs are hardly limited to cFFS. A variety of advanced sampling methods, including nonequilibrium umbrella sampling[47, 48] and metadynamics[49] have come across similar problems. One solution is to collapse the reaction coordinate to a single dimension using a string-type approach.[17, 42, 48] The string-type approach will prove difficult to implement in FFS without resorting to an iterative scheme requiring multiple FFS runs, because each path ensemble in FFS is generated sequentially and there is no opportunity to relax the string. Moreover, the string-type approach could defeat one of the benefits of cFFS, which is that it enables exploration of transitions with multiple tubes.

Extending cFFS to large numbers of CVs will thus require alternative approaches. Dimensionality reduction techniques such as isomaps[50, 51] or diffusion maps[52, 53] could be employed to reduce a large number of CVs to two or three reduced coordinates which capture the largest spread in the data. In this manner, multiple transition tubes would hopefully be preserved[33, 51] within the reduced coordinates. Furthermore, several groups are actively working to combine machine learning and advanced sampling methods to identify important CVs on-the-fly.[54–58] We are exploring if such methods or variations thereof can be incorporated with cFFS. One challenge to incorporating on-the-fly identification of reduced coordinates with FFS-type methods is again related to the sequential generation of ensembles. Sampling from the initial basin alone is unlikely to reveal reduced coordinates ideal for studying the transition. As FFS progresses, sampling from each interface ensemble will result in reduced coordinates which increasingly describe the transition. However, FFS requires that each ensemble be visited sequentially, and changing the definition of the reduced coordinates after each ensemble may cause substantial difficulty in maintaining this condition.

Studying rare events in simulations is an important and challenging problem that has spawned the development of many methods in the past decades. Here we restrict our comparison to two methods which use multiple CVs to sample, and calculate rate constants for rare transitions with unbiased dynamics in equilibrium or nonequilibrium systems. Vanden-Eijnden and Venturoli developed a method[59] that calculates the transition rate constants and transition paths from the steady state distribution under the boundary conditions that state  $A$  is a source and state  $B$  is a sink. The space between the stable states is tiled into enclosed Voronoi cells and parallel simulations are performed in each cell. The steady state flux and probability distribution can be estimated from the time spent in each cell and exchange between cells. Like cFFS, the method is applicable to equilibrium as well as nonequilibrium systems and does not require that  $A$  and  $B$  be well separated in both variables. Since each parallel path is restricted to a single cell, the method may prove advantageous compared with cFFS for systems with metastable intermediates. The method does not

provide direct access to dynamical transition paths, although, in principle, transition paths could probably be reconstructed with an extensive bookkeeping scheme. It is not immediately apparent which method would be better for systems with slowly decorrelating transition paths.

As mentioned in the introduction, Borrero and Escobedo[30] developed a method to optimize the FFS order parameter through a series of FFS runs. The approach uses committor information obtained from the prior FFS run to identify the best order parameter from a set of specified CVs. The procedure can be repeated until TPE sampling or the optimal order parameter converges. Like cFFS, the procedure in Ref. 30 allows FFS to be used in situations where there are a number of possible CVs. Since the FFS runs themselves are performed along a single order parameter (which may be a linear or nonlinear combination of multiple CVs), there is no limitation to the number of CVs which can be tested. For certain systems this may represent a substantial advantage over cFFS, which in current form is practically limited to three or four CVs. Unfortunately, the method presented in Ref. 30 requires multiple (often expensive) FFS runs. Additionally, given the sensitivity of FFS sampling to the choice of order parameter in the presence of multiple transition tubes, we suspect cFFS will perform better for such systems.

Lastly, we would like to comment on the possibility of combining a cFFS-type approach with other path sampling methods. At the most basic level, cFFS divides CV space into a fine grid to help define regions of phase space and interfaces between those regions with arbitrary shape. In cFFS, criteria for boundary identification were selected to meet the needs of FFS – a minimum number of total first crossings and constant average flux along the interface to avoid biasing the system to proceed in one direction over another. It is easy to imagine modifying the boundary identification criteria for other applications. Within the family of FFS approaches, it may prove fruitful to combine the approach of Borrero and Escobedo[30] with a cFFS-type approach for interface definitions. This could allow interfaces with any arbitrary shape which could better reproduce the committor function. Transition interface sampling is less sensitive to the definition of order parameter.[25, 26] However, a procedure has been proposed to optimize interface placement given the order parameter.[60] This criterion for optimal interface placement could be combined with a cFFS-type approach for dividing the CV space for transition interface sampling.

## VII. CONCLUDING REMARKS

We described cFFS, a method to sample rare event transitions along multiple CVs simultaneously. cFFS uses automated nonlinear interface placement and reveals on-the-fly the evolution of CVs during a transition. cFFS was tested with two CVs, but in principle, it can be extended to three or more. In practice, extending cFFS in current form to more than three or four CVs may prove challenging. The stable states only need to be separated in a combination of CVs, which may change nonmonotonically between the stable states. We introduced a criterion of constant flux along each interface to prevent biasing TPE. cFFS results in correct estimates of the transition rate constants and TPE sampling on several 2D PESs and the  $C_{7ax}$ -to- $C_{7eq}$  transition in alanine dipeptide in vacuum. We additionally demonstrated cFFS on 1D analytical potential using one position coordinate and one momenta coordinate. cFFS substantially improved upon FFS results on the same potential, where only the position coordinate was used as the order parameter. On the 2D PESs, cFFS performed particularly well for systems with hysteresis or multiple transition tubes. cFFS with multiple suboptimal order parameters consistently outperformed FFS with a single suboptimal order parameter. Since optimal order parameters are not known in most applications of FFS, cFFS with two or more suboptimal order parameters will be beneficial for studies of complex systems such as macromolecular conformational transitions and crystal nucleation.

## ACKNOWLEDGMENTS

We thank the referees for thoughtful suggestions which substantially improved an earlier version of this work. This material is based upon work supported by the U.S. Department of Energy, Office of Science, Office of Basic Energy Sciences, under Award Number de-sc0015448. Clemson University is acknowledged for generous allotment of compute time on the Palmetto cluster.

**Supporting Information Available:** Details of Langevin dynamics, PESs, TPE sampling at  $\beta = 2.5$ , FFS/cFFS sampling on PES-3 at  $\beta = 5.0$ , and details of alanine dipeptide simulations.

- 
- [1] B. Peters, *Reaction Rate Theory and Rare Events* (Elsevier, 2017).
- [2] Y. Bi and T. Li, *J. Phys. Chem. B* **118**, 13324 (2014).
- [3] A. Haji-Akbari, R. S. DeFever, S. Sarupria, and P. G. Debenedetti, *Phys. Chem. Chem. Phys.* **16**, 25916 (2014).
- [4] A. Haji-Akbari and P. G. Debenedetti, *Proc. Natl. Acad. Sci. USA* **112**, 10582 (2015).
- [5] R. S. DeFever and S. Sarupria, *J. Chem. Phys.* **147**, 204503 (2017).
- [6] P. L. Geissler, C. Dellago, and D. Chandler, *J. Phys. Chem. B* **103**, 3706 (1999).



- [7] E. Pluhařová, M. D. Baer, G. K. Schenter, P. Jungwirth, and C. J. Mundy, *J. Phys. Chem. B* **120**, 1749 (2015).
- [8] J. Juraszek and P. G. Bolhuis, *Proc. Natl. Acad. Sci. USA* **103**, 15859 (2006).
- [9] C. Velez-Vega, E. E. Borrero, and F. A. Escobedo, *J. Chem. Phys.* **133**, 105103 (2010).
- [10] M. Moqadam, A. Lervik, E. Riccardi, V. Venkatraman, B. K. Alsborg, and T. S. van Erp, *Proc. Natl. Acad. Sci. USA* **115**, E4569 (2018).
- [11] C. H. Bennett, “Molecular dynamics and transition state theory: The simulation of infrequent events,” in *Algorithms for Chemical Computations*, Chap. 4, pp. 63–97.
- [12] C. Dellago, P. G. Bolhuis, F. S. Csajka, and D. Chandler, *J. Chem. Phys.* **108**, 1964 (1998).
- [13] W. E, W. Ren, and E. Vanden-Eijnden, *Phys. Rev. B* **66**, 052301 (2002).
- [14] T. S. van Erp, D. Moroni, and P. G. Bolhuis, *J. Chem. Phys.* **118**, 7762 (2003).
- [15] R. J. Allen, P. B. Warren, and P. R. ten Wolde, *Phys. Rev. Lett.* **94**, 018104 (2005).
- [16] R. J. Allen, D. Frenkel, and P. R. ten Wolde, *J. Chem. Phys.* **124**, 024102 (2006).
- [17] L. Maragliano, A. Fischer, E. Vanden-Eijnden, and G. Ciccotti, *J. Chem. Phys.* **125**, 024106 (2006).
- [18] T. S. van Erp, *Phys. Rev. Lett.* **98**, 268301 (2007).
- [19] P. Tiwary and M. Parrinello, *Phys. Rev. Lett.* **111**, 230602 (2013).
- [20] H. Jung, K. Okazaki, and G. Hummer, *J. Chem. Phys.* **147**, 152716 (2017).
- [21] P. G. Bolhuis and C. Dellago, “Trajectory-based rare event simulations,” in *Reviews in Computational Chemistry* (Wiley-Blackwell, 2010) Chap. 3, pp. 111–210.
- [22] In this work, a *collective variable* is a quantity that can be calculated from the configuration space coordinates of the system. An *order parameter* is a collective variable that can distinguish between states *A* and *B*.
- [23] R. J. Allen, C. Valeriani, and P. R. ten Wolde, *J. Phys. Condens. Mat.* **21**, 463102 (2009).
- [24] F. A. Escobedo, E. E. Borrero, and J. C. Araque, *J. Phys. Condens. Mat.* **21**, 333101 (2009).
- [25] T. S. van Erp, *J. Chem. Phys.* **125**, 174106 (2006).
- [26] T. S. van Erp, “Dynamical rare event simulation techniques for equilibrium and nonequilibrium systems,” in *Kinetics and Thermodynamics of Multistep Nucleation and Self Assembly in Nanoscale Materials* (Wiley-Blackwell, 2012) Chap. 2, pp. 27–60.
- [27] J. Juraszek and P. G. Bolhuis, *Biophys. J.* **95**, 4246 (2008).
- [28] C. Velez-Vega, E. E. Borrero, and F. A. Escobedo, *J. Chem. Phys.* **130**, 225101 (2009).
- [29] G. C. Sosso, T. Li, D. Donadio, G. A. Tribello, and A. Michaelides, *J. Phys. Chem. Lett.* **7**, 2350 (2016).
- [30] E. E. Borrero and F. A. Escobedo, *J. Chem. Phys.* **127**, 164101 (2007).
- [31] J. Russo and H. Tanaka, *J. Chem. Phys.* **145**, 211801 (2016).
- [32] M. A. Rohrdanz, W. Zheng, and C. Clementi, *Ann. Rev. Phys. Chem.* **64**, 295 (2013).
- [33] S. B. Kim, C. J. Dsilva, I. G. Kevrekidis, and P. G. Debenedetti, *J. Chem. Phys.* **142**, 085101 (2015).
- [34] T. S. Van Erp and P. G. Bolhuis, *J. Comput. Phys.* **205**, 157 (2005).
- [35] A. Vijaykumar, P. R. ten Wolde, and P. G. Bolhuis, *J. Chem. Phys.* **148**, 124109 (2018).
- [36] J. Lin, *IEEE T. Inform. Theory* **37**, 145 (1991).
- [37] C. Leitold, W. Lechner, and C. Dellago, *J. Phys. Condens. Mat.* **27**, 194126 (2015).
- [38] R. B. Best and G. Hummer, *Proc. Natl. Acad. Sci. USA* **102**, 6732 (2005).
- [39] A. Ma and A. R. Dinner, *J. Phys. Chem. B* **109**, 6769 (2005).
- [40] B. Peters and B. L. Trout, *J. Chem. Phys.* **125**, 054108 (2006).
- [41] A. Singer, R. Erban, I. G. Kevrekidis, and R. R. Coifman, *Proc. Natl. Acad. Sci. USA* **106**, 16090 (2009).
- [42] W. Lechner, J. Rogal, J. Juraszek, B. Ensing, and P. G. Bolhuis, *J. Chem. Phys.* **133**, 174110 (2010).
- [43] W. Li and A. Ma, *Mol. Simul.* **40**, 784 (2014).
- [44] B. Peters, *Ann. Rev. Phys. Chem.* **67**, 669 (2016).
- [45] D. Mendels, G. Piccini, and M. Parrinello, *J. Phys. Chem. Lett.* **9**, 2776 (2018).
- [46] P. G. Bolhuis, C. Dellago, and D. Chandler, *Proc. Natl. Acad. Sci. USA* **97**, 5877 (2000).
- [47] A. Warmflash, P. Bhimalapuram, and A. R. Dinner, *J. Chem. Phys.* **127**, 154112 (2007).
- [48] A. Dickson, A. Warmflash, and A. R. Dinner, *J. Chem. Phys.* **130**, 074104 (2009).
- [49] A. Laio and M. Parrinello, *Proc. Natl. Acad. Sci. USA* **99**, 12562 (2002).
- [50] J. B. Tenenbaum, V. De Silva, and J. C. Langford, *Science* **290**, 2319 (2000).
- [51] P. Das, M. Moll, H. Stamati, L. E. Kaviraki, and C. Clementi, *Proc. Natl. Acad. Sci.* **103**, 9885 (2006).
- [52] R. R. Coifman, S. Lafon, A. B. Lee, M. Maggioni, B. Nadler, F. Warner, and S. W. Zucker, *Proc. Natl. Acad. Sci. USA* **102**, 7426 (2005).
- [53] A. L. Ferguson, A. Z. Panagiotopoulos, I. G. Kevrekidis, and P. G. Debenedetti, *Chem. Phys. Lett.* **509**, 1 (2011).
- [54] E. Chiavazzo, R. Covino, R. R. Coifman, C. W. Gear, A. S. Georgiou, G. Hummer, and I. G. Kevrekidis, *Proc. Natl. Acad. Sci. USA* **114**, E5494 (2017).
- [55] W. Chen and A. L. Ferguson, *J. Comput. Chem.* **39**, 2079 (2018).
- [56] J. M. L. Ribeiro, P. Bravo, Y. Wang, and P. Tiwary, *J. Chem. Phys.* **149**, 072301 (2018).
- [57] M. M. Sultan and V. S. Pande, *J. Chem. Phys.* **149**, 094106 (2018).
- [58] C. Wehmeyer and F. Noé, *J. Chem. Phys.* **148**, 241703 (2018).
- [59] E. Vanden-Eijnden and M. Venturoli, *J. Chem. Phys.* **131**, 044120 (2009).
- [60] E. E. Borrero, M. Weinwurm, and C. Dellago, *J. Chem. Phys.* **134**, 244118 (2011).

**Supporting Information: Contour forward flux sampling: Sampling rare events  
along multiple collective variables**

Ryan S. DeFever and Sapna Sarupria\*  
*Department of Chemical & Biomolecular Engineering  
Clemson University, Clemson, SC 29634*

arXiv:1901.03422v1 [cond-mat.stat-mech] 10 Jan 2019

---

\* [ssarupr@g.clemson.edu](mailto:ssarupr@g.clemson.edu)

TABLE S1: Barrier heights for PESs. TS1 and TS2 are the positive- $y$  and negative- $y$  transition states, respectively.

	$A \xrightarrow{\text{TS1}} B$	$A \xrightarrow{\text{TS2}} B$
PES-1	3.402	N/A
PES-2	3.403	N/A
PES-3	3.403	3.403
PES-4	3.405	4.143

## S1. DETAILS OF LANGEVIN DYNAMICS AND FFS/CFFS PARAMETERS

The behavior of a particle on the four potential energy surfaces (PESs) was described by the Langevin equation,  $\ddot{\mathbf{q}} = -\nabla U(\mathbf{q}) - \gamma \dot{\mathbf{q}} + \sqrt{2\gamma k_B T} R(t)$ , where  $\mathbf{q}$  represents the coordinates of the particle,  $U(\mathbf{q})$  is the PES,  $\gamma$  is the friction coefficient,  $k_B$  is the Boltzmann constant,  $T$  is the reduced temperature, and  $R(t)$  is delta-correlated Gaussian random noise with zero mean and unit variance. The dynamics were generated with the velocity Verlet integrator with a time step of 0.01. Simulations were performed at  $\gamma = 5.0$ . We confirmed that  $\gamma = 5.0$  provides sufficient stochasticity for FFS by comparing rates estimated from straightforward Langevin dynamics (SLD) with rates estimated from FFS for a range of  $\gamma$  from 0.01 to 100 at  $\beta = 2.5$  (data not reported). FFS rates agreed with SLD for all surfaces at  $\gamma \geq 1.0$ . At  $\gamma < 1.0$  FFS underestimated the rate constant. It is possible that  $\gamma = 5.0$  does not provide sufficient stochasticity at  $\beta = 5.0$ . This may explain why FFS<sub>opt</sub> and cFFS rates at  $\beta = 5.0$  agree more closely with SLD for surfaces with a more flatter and thus more diffusive transition region (PES-1 and PES-4).

SLD results were averaged over 50 and 400-600 independent simulations of length  $10^7$  time units at  $\beta = 2.5$  and  $\beta = 5.0$ , respectively. FFS/cFFS results were averaged from three independent trials. At  $\beta = 2.5$ , FFS/cFFS was performed with 10,000 trajectories per interface at 1,000 configurations per interface. At  $\beta = 5.0$ , FFS/cFFS was performed with 40,000 trajectories per interface and 4,000 configurations per interface.

## S2. POTENTIAL ENERGY SURFACES

Equations for the PESs used in this work are reported in Eqns. 1–4. Barrier heights are provided in Table S1. For each surface, the negative- $x$  minimum is considered state  $A$  and the positive- $x$  minimum state  $B$ . The potential energy difference from the minimum of  $A$  to the lowest potential energy transition state is 3.4 for all surfaces. PES-1 and PES-2 have a single transition tube, while PES-3 and PES-4 have two transition tubes.

$$V_{\text{PES-1}}(x, y) = 0.02(x^4 + y^4) - 4 \exp(-((x+2)^2 + (y+2)^2)) - 4 \exp(-((x-2)^2 + (y-2)^2)) + 0.3(x-y)^2 + 0.0026 \quad (1)$$

$$V_{\text{PES-2}}(x, y) = 0.02(x^2 + y^2)^2 - 5.196 \exp(-0.08(x+3.5)^2 - 1.5(y+1.3)^2) - 5.196 \exp(-0.08(x-3.5)^2 - 1.5(y-1.3)^2) + 0.30914 \quad (2)$$

$$V_{\text{PES-3}}(x, y) = 0.02(x^4 + y^4) - 3.73 \exp(-((x+2)^2/8 + (y+2)^2/8)) - 3.73 \exp(-((x-2)^2/8 + (y-2)^2/8)) + 3 \exp(-x^2/2 + y^2/15) + 2 \exp(-x^2/2 + y^2/2) - 0.5085 \quad (3)$$

$$V_{\text{PES-4}}(x, y) = -2.93 \exp(-((x-3)^2/2 + (y-2.5)^2/2)) - 2.93 \exp(-((x+2)^2/2 + (y+2)^2/2)) + 3 \exp(-0.32((x+1)^2 + (y-2)^2 + 12(x+y-2.7)^2 - 1)) + 6 \exp(-0.15((x-2)^2 + (y-1)^2 + 10(x+y)^2 - 1)) + 0.005(x^4 + y^4) - 0.627 \quad (4)$$

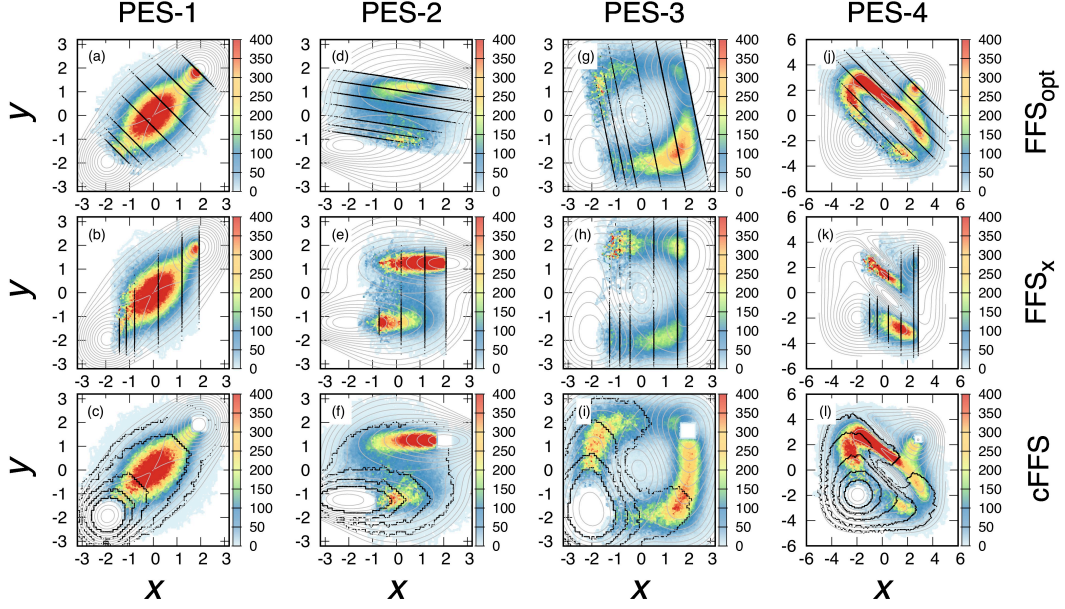


FIG. S1: Comparison of interface placement and TPE sampling generated with  $\text{FFS}_{\text{opt}}$ ,  $\text{FFS}_x$ , and cFFS on PES-1 – PES-4 at  $\beta = 2.5$ . PES contours are shown as gray lines. Configurations at each interface are shown with black points. TPE sampling is represented by the heat map.

### S3. TPE SAMPLING AT $\beta = 2.5$

Transition path ensemble (TPE) sampling at  $\beta = 2.5$  is reported in Fig. S1. All methods result in similar sampling to the SLD results reported in Fig. 1 of the main text. All methods successfully sample both transition tubes for PES-3 and PES-4 at this higher temperature.

### S4. FFS SAMPLING ON PES-3 AT $\beta = 5.0$

FFS struggles to sample both transition tubes at  $\beta = 5.0$  on PES-3. TPE sampling for all three runs of FFS with three different order parameters and cFFS are reported in Fig. S2. Even with the optimal order parameter  $(5x + y)$ , FFS fails to equally sample both transition tubes. With one suboptimal order parameter  $(x + y)$  FFS always samples the positive- $y$  transition tube, while with a different suboptimal order parameter  $(x)$ , FFS always samples the negative- $y$  transition tube. cFFS consistently samples both transition tubes.

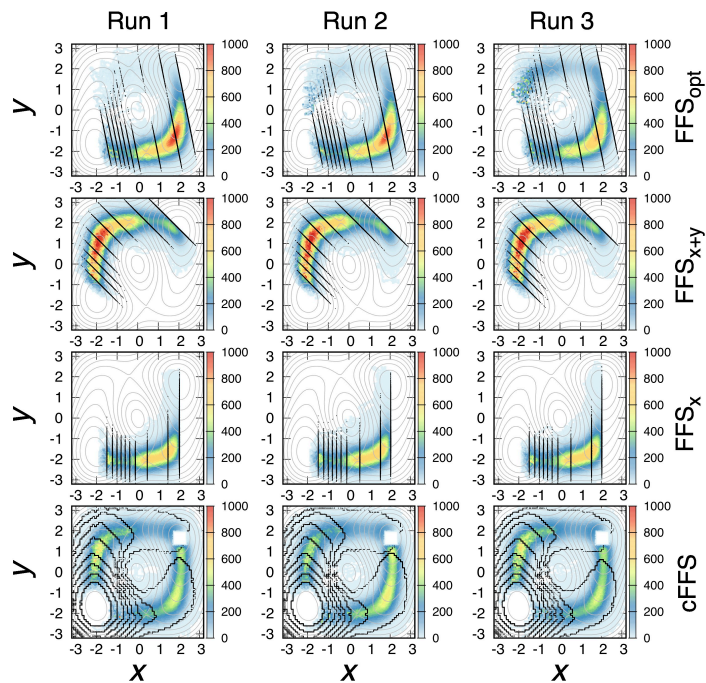


FIG. S2: Comparison of interface placement and TPE sampling generated with FFS<sub>opt</sub>, FFS<sub>x+y</sub>, FFS<sub>x</sub>, and cFFS on PES-3 at  $\beta = 5.0$ . Results are shown for all three independent FFS runs for each method. PES contours are shown as gray lines. Configurations at each interface are shown with black points. TPE sampling is represented by the heat map.

## S5. DETAILS OF ALANINE DIPEPTIDE SIMULATIONS

Alanine dipeptide was simulated in vacuum with Langevin dynamics at 300 K with the leap-frog stochastic dynamics integrator implemented in GROMACS 2018.[1] The integration time step was 0.002 ps and  $\gamma = 100 \text{ ps}^{-1}$ . Linear and angular center of mass motion was removed every step. Alanine dipeptide was represented with the AMBER99SB force field.[2] Bonds between heavy atoms and a hydrogen were constrained with LINCS.[3, 4]

cFFS was tested by investigating the  $C_{7\text{ax}}\text{-to-}C_{7\text{eq}}$  conformational transition, which requires surmounting an  $\sim 10 k_B T$  barrier.[5] The SLD rate constant was estimated from 25 independent simulations. Each simulation was initiated from the  $C_{7\text{ax}}$  basin located near  $\phi = 60^\circ$  and  $\psi = -30^\circ$ . Following an energy minimization, the systems were equilibrated for 1 ns prior to the start of the production runs. Each production run was continued until the system committed to the  $C_{7\text{eq}}$  basin or for a maximum of 500 ns. 23 of the 25 simulations underwent the conformational transition within 500 ns. The rate constant was estimated as  $k_{AB} = n_{AB}/t_A$  where  $n_{AB}$  is the number of  $C_{7\text{ax}}\text{-to-}C_{7\text{eq}}$  transitions and  $t_A$  is the total simulation time spent in the  $C_{7\text{ax}}$  basin, and thus  $k_{AB}^{\text{SLD}} = 4.8 \times 10^6 \text{ s}^{-1}$ .

cFFS was performed for the same system. Simulation in basin  $A$  was initiated from an energy minimized configuration in the  $C_{7\text{ax}}$  basin. The system was equilibrated for 1 ns prior to the start of a 10 ns production simulation.  $\phi$  and  $\psi$  were selected as the CVs for cFFS. The grid extended from  $-180^\circ$  to  $180^\circ$  in both  $\phi$  and  $\psi$  with periodic boundaries. A grid size of  $2^\circ$  was used in both  $\phi$  and  $\psi$ . The bounds of basin  $B$  were defined by examining the free energy landscape reported in the Supporting Information of Ref. 5. The bounds of basin  $A$  were identified with a threshold probability density of  $4.0 \times 10^{-4}$ . This results in the system spending  $\sim 60\%$  of the time within the bounds of  $A$  during the basin simulation. The flux from  $A$  to  $\lambda_0$  was calculated to be  $6.15 \times 10^{10} \text{ s}^{-1}$ . Atomic velocities were *not* regenerated at the shooting points as the stochastic dynamics allowed individual trajectories to diverge. Complete details of the cFFS run are reported in Table S2. The total probability of reaching  $B$  from  $\lambda_0$  is  $\sum_{i=0}^4 P(\lambda_B|\lambda_i)P(\lambda_i|\lambda_0) = 8.15 \times 10^{-5}$  and thus  $k_{AB}^{\text{cFFS}} = 5.0 \times 10^6 \text{ s}^{-1}$ .

TABLE S2: Alanine dipeptide cFFS details

$i$	$N_{\text{conf}}$	$N_{\text{basin}}$	$N_{\text{cross}}$	$N_{\text{succ}}$	$N_{\text{total}}$	$P(\lambda_{i+1} \lambda_i)$	$P(\lambda_i \lambda_0)$	$P(\lambda_B \lambda_i)$
0	615	9347	653	0	10000	0.0653	1.0	0.0
1	653	9394	606	0	10000	0.0606	$6.53 \times 10^{-2}$	0.0
2	606	9397	586	17	10000	0.0586	$3.96 \times 10^{-3}$	0.0017
3	582	6471	466	3063	10000	0.0466	$2.32 \times 10^{-4}$	0.3063
4	466	3258	0	1742	5000	0.0	$1.08 \times 10^{-5}$	0.3484

- 
- [1] M. J. Abraham, T. Murtola, R. Schulz, S. Páll, J. C. Smith, B. Hess, and E. Lindahl, *SoftwareX* **1-2**, 19 (2015).  
[2] V. Hornak, R. Abel, A. Okur, B. Strockbine, A. Roitberg, and C. Simmerling, *Proteins* **65**, 712 (2006).  
[3] B. Hess, H. Bekker, H. J. C. Berendsen, and J. G. E. M. Fraaije, *J. Comput. Chem.* **18**, 1463 (1997).  
[4] B. Hess, *J. Chem. Theory Comput.* **4**, 116 (2008).  
[5] D. Mendels, G. Piccini, and M. Parrinello, *J. Phys. Chem. Lett.* **9**, 2776 (2018).